BREAKOUT RECONNECTION OBSERVED BY THE TESIS EUV TELESCOPE

REVA A.A., ULYANOV A.S., SHESTOV S.V., KUZIN S.V. Lebedev Physical Institute, Russian Academy of Sciences

Draft version August 6, 2018

Abstract

We present experimental evidence of the coronal mass ejection (CME) breakout reconnection, observed by the TESIS EUV telescope. The telescope could observe solar corona up to 2 R_{\odot} from the Sun center in the Fe 171 Å line. Starting from 2009 April 8 TESIS, observed an active region (AR) that had a quadrupolar structure with an X-point 0.5 R_{\odot} above photosphere. A reconstructed from the MDI data magnetic field also has a multipolar structure with an X-point above the AR. At 21:45 UT on April 9, the loops near the X-point started to move away from each other with a velocity of \approx 7 km s⁻¹. At 01:15 UT on April 10, a bright stripe appeared between the loops, and the flux in the GOES 0.5–4 Å channel increased. We interpret the loops' sideways motion and the bright stripe as evidence of the breakout reconnection. At 01:45 UT, the loops below the X-point started to slowly move up. At 15:10 UT, the CME started to accelerate impulsively, while at the same time a flare arcade formed below the CME. After 15:50 UT, the CME moved with constant velocity. The CME evolution precisely followed the breakout model scenario.

Keywords: Sun: corona—Sun: coronal mass ejections (CMEs)

1. INTRODUCTION

Coronal mass ejections (CMEs) are giant eruptions of coronal plasma into interplanetary space. CMEs are the result of an energy release in the corona and are one of the major factors that affect space weather (Schwenn 2006; Pulkkinen 2007). Investigation of CMEs are important for solar physics and questions of solar-terrestrial connections.

According to the standard CME model, before eruption, the CME has a bipolar magnetic field structure with a prominence above it (Carmichael 1964; Sturrock 1966; Hirayama 1974; Kopp & Pneuman 1976). The prominence is surrounded by circular magnetic field lines. Under the prominence, there is a current sheet in which reconnection happens. Plasma outflow from the reconnection region pushes the prominence up and the CME erupts.

In a bipolar configuration, when a CME erupts, all overlying loops should open up (that is, reconnect to infinity) and free the way for the CME. Aly (1984) and Sturrock (1991) showed that, in this case, the final open magnetic configuration has more energy than the initial closed configuration. So, with respect to energy, eruption is impossible. This contradiction is known as the Aly-Sturrock limit.

To resolve the Aly-Sturrock limit, Antiochos et al. (1999) proposed a 'breakout model' of CME, in which overlying loops remain closed after the eruption. In the breakout model, an arcade is confined by a quadrupolar magnetic structure (see Figure 1a). The arcade experiences slow shearing motion. The shearing motion pumps into the arcade non-potential magnetic energy, which is needed for an eruption. The reconnection in the X-point of the quadrupolar structure is so slow that it allows to store magnetic energy in the sheared arcade. Eventually, the X-point stretches into the current sheet, and

overlying loops reconnect (see Figure 1a). This external reconnection—which is called the breakout reconnection—removes overlying flux above the X-point and sends it to the side. The breakout reconnection relieves magnetic tension and allows the sheared structure to rise. The CME slowly moves up (see Figure 1b). The motion stretches the current sheet below the CME, and flare reconnection occurs (see Figure 1c). Plasma outflow from the reconnection region pushes the CME up, and the CME impulsively accelerates and erupts (see Figure 1d). In the breakout model, the overlying loops remain closed after eruption and, therefore, the Aly-Sturrock limit is not violated.

The breakout model has been extensively studied with numerical magnetohydrodynamic (MHD) simulations. The first complete simulation of breakout CME evolution was performed by MacNeice et al. (2004). The first 3D simulation of breakout CME was performed by Lynch et al. (2005). Karpen et al. (2012) performed a high-resolution MHD simulation of the breakout model and reproduced all aspects of the model described in the previous paragraph.

Several events showed indirect evidence of the breakout model: quadrupolar magnetic field structure of the Bastille day flare (Aulanier et al. 2000); 'EIT crinckles' (Sterling & Moore 2001); dimmings before the CME (Sterling & Moore 2004a); CME quadrupolar magnetic structure inferred from SXT images (Sterling & Moore 2004b); timing of brightenings during CME (Gary & Moore 2004); and prominence location relative to hotter plasma in the CME (Reva et al. 2014). Manoharan & Kundu (2003); Aurass et al. (2011, 2013) reported radio sources above null points of the CME quadrupolar structure before eruption, which the authors interpreted as evidence of breakout reconnection. However, despite the success of the breakout model, its key element—the breakout reconnection—was never directly observed.

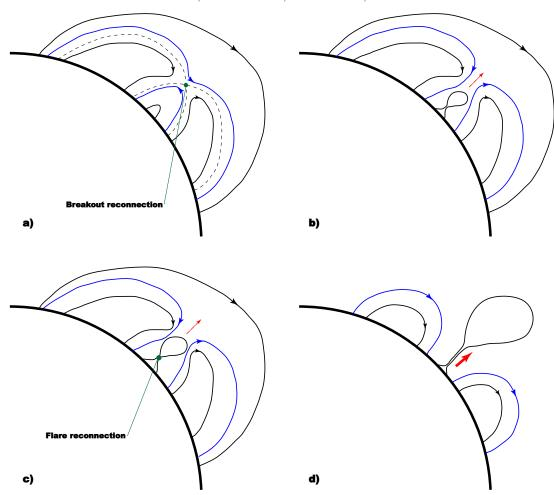


Figure 1. Breakout model: a) breakout reconnection; b) CME slowly moves up; c) flare reconnection; d) impulsive acceleration. Thick black line—solar surface; thin black lines—magnetic field lines; blue lines—reconnecting magnetic field lines.

The breakout magnetic structure is expected to be large. Its X-point should be located at a distance of $1.2-2~R_{\odot}$ from the Sun's center (we will call this distance range 'far corona'). To confirm the breakout model, we need observations in the far corona. Although instruments that could observe far corona existed—LASCO/C1 coronograph (Zhang et al. 2001), Siberian solar radio telescope (Alissandrakis et al. 2013), Mauna Loa Observatory (Bemporad et al. 2007), TESIS EUV telescopes (Reva et al. 2014), and SWAP EUV telescope (Seaton et al. 2013)—they were never used to test the breakout model.

One of the TESIS EUV telescopes observed far corona in 171 Å (Kuzin et al. 2011). Solar corona images in the 171 Å line show individual coronal loops, and therefore, could reveal coronal magnetic structure. In this work, we present TESIS CME observations in the 171 Å line, which, for the first time, directly showed evidence of the breakout reconnection.

2. EXPERIMENTAL DATA

We analyzed CME that occurred on 2009 April 10. We used the TESIS 171 Å telescope data to study CME behavior below 2 R_{\odot} , and the LASCO/C2, C3 data above 2 R_{\odot} . We also used STEREO-A EUVI images to observe CME evolution behind the limb, and COR2 images to

study the CME kinematics. We used MDI data for the reconstruction of the magnetic field.

TESIS is an instrument assembly that observed the solar corona in EUV and soft X-ray. It worked on board the CORONAS-PHOTON satellite in 2009 (Kotov 2011). TESIS included an EUV telescope, which built solar corona images in the Fe 171 Å line with 1.7" angular resolution and 1° field of view. For the Fe 171 Å telescope, a special observational program was developed, in which the telescope built images of far corona (for more details, see Reva et al. 2014). From April 8 to 10, TESIS worked in the far corona mode with a varying cadence of 10, 20, and 30 minutes. We used TESIS 171 Å telescope data to study CME behavior below 2 R_{\odot} .

LASCO is a set of coronographs that observe solar corona in white light (Brueckner et al. 1995). LASCO works on the SOHO satellite (Domingo et al. 1995). LASCO coronographs cover different distance ranges: C1 1.1–3 R_{\odot} ; C2 2–6 R_{\odot} ; and C3 4–30 R_{\odot} . LASCO/C1 stopped operating in 1998, and today corona below 2 R_{\odot} is a 'blind zone' for LASCO. We use LASCO data to complement TESIS data at distances above 2 R_{\odot} .

STEREO is a set of two satellites that move along the Earth's orbit: STEREO-A moves ahead of the Earth and STEREO-B moves behind it (Howard et al. 2008). STEREO carries Extreme UltraViolet Imager (EUVI),

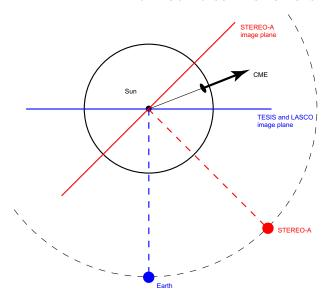


Figure 2. STEREO-A, Earth, and CME positions.

which builds solar corona images in 171, 195, 284, and 304 Å lines. We use STEREO-A EUVI images to observe early CME evolution behind the solar limb.

STEREO also carries two coronagraphs: COR1 and COR2. COR1 builds corona white light images at a distance range of 1.3–4 R_{\odot} and COR2 at 2–15 R_{\odot} . Due to the gap in the observations, COR1 did not observed the studied CME and COR2 observed it above 4 R_{\odot} . We use COR2 data to study the CME kinematics.

On 2009 April 10 STEREO-A was 46° ahead of the Earth (see Figure 2). The active region(AR) was behind the limb, and the CME trajectory was inclined by approximately the same angle to the TESIS and STEREO-A image planes.

The Michelson Doppler Imager (MDI, Scherrer et al. (1995)) works on the *SOHO* satellite. In a synoptic mode, MDI maps the line-of-sight component of the photospheric magnetic field with a 4" resolution and 90-minutes cadence. We used MDI data to reconstruct the magnetic field.

3. RESULTS

3.1. TESIS Observations

We studied an AR, which appeared above the eastern limb in the northern hemisphere on 2009 March 26, and crossed the western limb on 2009 April 8. The AR could be traced further with *STEREO-A* EUVI telescopes. In 2009, the Sun was in the deep minimum of the solar activity and the analyzed AR was very weak. It did not have any sunspots and was not classified by NOAA.

The TESIS EUV telescope observed this AR in the far corona mode beginning on April 8, 12:00 UT. At this time, the AR was already at the western limb and TESIS could see its far corona structure.

In TESIS 171 Å images before eruption, the analyzed AR had a quadrupolar structure with a size of ≈ 750 Mm (see Figure 3). Although it is hard to distinguish the AR structure on a single image, an inspection of the video for Figure 7 allows us to distinguish individual loops, their dynamics, and point them on individual images. The X-point of the magnetic structure was located at the height

of $\approx 0.5 R_{\odot} (\approx 350 \text{ Mm})$ above the photosphere.

Figure 4 shows a zoomed image of the X-point. To highlight the X-point, we used a multicolor color table. Although the inferred X-point is not fully revealed in this Figure, we can see the connected apexes of the north and the south loops of the quadrupolar system. We can also see that these apexes started to diverge from each other.

On 2009 April 9, at 21:45 UT, loops near the X-point started to move away from each other (see Figure 3 and 4). On 2009 April 10, at 01:15 UT, a bright stripe (80 Mm in length) appeared between the loops (see Figure 3 and the video for Figure 7). We interpreted the loops' motions and the bright stripe as evidence of the breakout reconnection.

We measured the time dependence of distance between loops, which formed the X-point (see Figure 5). The measurement was carried out manually with a simple point-and-click method. To estimate error bars, we repeated the procedure 25 times. The loops moved away from each other at a speed of ≈ 7 km s⁻¹. When the bright stripe appeared, the movement stopped for ≈ 3 hours, and the flux in GOES the 0.5–4 Å channel increased (see Figure 5). When the bright stripe disappeared, the movement continued.

To illustrate the loops' motion more clearly, we made a stack plot of slices, cut from the TESIS images in the vicinity of the X-point (see Figure 6). The position of the slices is shown in Figure 3. During the evolution, the bright stripe slightly moved up. We moved the position of the slices to follow the vertical motion of the bright stripe.

In Figure 6, the upper bright feature (y=190 Mm, t=00:00 UT) corresponds to the apex of the north loop, and the bottom bright feature (y=110 Mm, t=00:00 UT) corresponds to the apex of the south loop. 21:45 UT these loops touched each other and formed an X-point. From 21:45 to 01:15 UT, the loops diverged from each other. Both loops started to move simultaneously. We interpret this motion as a restructuring of the magnetic field (evidence of the breakout reconnection). From 01:15 to 04:15 UT, the bright stripe lightens up between the loops. The stripe resembled the current sheet, and we interpret it as another evidence of the breakout reconnection. An apparent converging motion of the bright features (starting from 03:15 UT) is not a loop motion, but a shift of the bright stripe intensity maximum from the north to the south loop.

Starting at 03:15 UT, the structures are more blurred, and it is harder to identify loop apexes. The pause in the loop divergence motion reported above could be a result of a subjective mistake in the identification of the blurred loop apexes.

The bright stripe intensity on the TESIS images was 160 DNs, the coronal hole intensity was 1010 DNs, and the quiet Sun intensity was 4120 DNs. So, the bright stripe intensity amounted to 15 % of the coronal hole intensity or 4 % of the quiet Sun intensity. On the STEREO-A images, quiet Sun intensity was 700 DNs but the bright stripe was not seen. Its intensity should be around 30 DNs. Most likely, we did not observe the bright stripe on the EUVI-A images due to its low intensity, or because the corresponding EUVI-A line of sight is on-disk and thus intercepts denser layers.

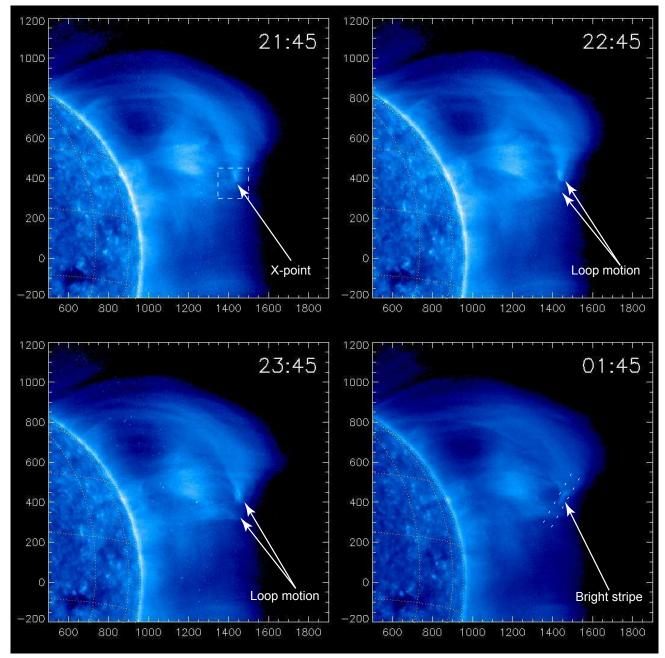


Figure 3. Reconnection of the overlying loop. The dashed lines indicate the position and the width of the slices, which were used in the construction of the Figure 6. The dashed rectangle shows the field of view of Figure 4. Images were taken on April 9, 2009. Coordinates are measured in arc seconds.

On 2009 April 10, at 15:00 UT, the CME erupted (see Figure 7). It had a loop-like shape. We measured coordinates of the CME's leading edge on the TESIS and LASCO images. The CME moved with almost constant velocity of $\approx 165~\rm km~s^{-1}$. When the CME erupted, its footpoints were behind the limb, so we did not see CME acceleration on the TESIS images.

3.2. Magnetic Field

We assumed above that the observed structure had a 2D magnetic field configuration, which could be incorrect. In that case, more complex 3D models should be adopted.

In order to prove the correspondence between the field

configuration in the breakout model (Figure 1) and the actual magnetic topology, we reconstructed the field in a potential approximation using MDI data. The magnetogram of the AR obtained on 2009 April 2, is presented in Figure 8. As we can see, the AR is bipolar and no other strong AR was observed. The only unaccounted for source of the observed 'quadrupolarity' is the global magnetic field of the Sun. We suggest that the two missing poles represent the north and south poles of the Sun. This assumption is justified because the studied AR was the only existing large-scale bipole on the Sun.

To check this assumption, we applied the Potential Field Source Surface model (PFSS, Mackay & Yeates 2012), which is based on the spherical harmonic decom-

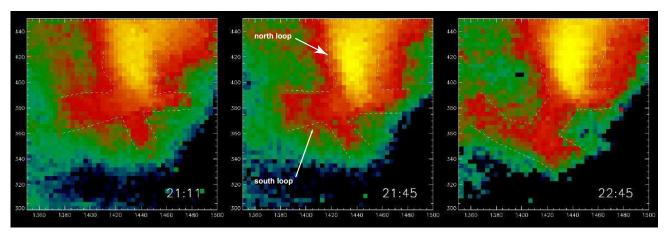


Figure 4. Breakout X-point, observed by TESIS (a zoomed version of the Figure 3). Blue and green correspond to low intensities; red and yellow correspond to high intensities. Contours denote the X-point. Arrows indicate the north and south loops of the quadrupolar structure. Images were taken on 2009 April 9. Coordinates are measured in arc seconds.

position of the field. The required input parameter to this model is the value of the radial component of the field on the photosphere. Because it is impossible to measure the field throughout the whole solar surface at one time, we used a field map 'stitched' from multiple MDI magnetograms scanned during the current solar rotation. PFSS has a single free parameter—the height of the source surface, i.e., the distance at which field potential is set to zero. For our modeling, we took the standard value of 2.5 solar radii.

The reconstructed magnetic field is shown in Figure 9. The notable feature of this configuration is a coronal null-point created by the positive source of AR and the south pole, which is situated at a height of approximately 120 Mm above the surface. The field lines adjacent to the null-point are blue in the images. The separator field line (shown in red) originating from the null divides the overall flux into four major domains connecting four given sources. Figure 9 shows only part of the separator, which connects the null-point and the highest point of the arcade.

The 3D field highly resembles the breakout model. The only significant difference is the X-point being substituted by the separator. Moreover, the side view of the 3D field almost perfectly fits the TESIS images (see Fig-

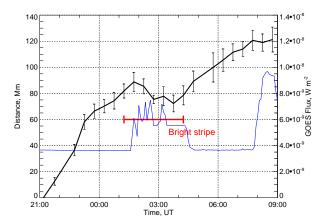


Figure 5. Distance between the loops, which formed the breakout X-point. Red indicates the time when the bright stripe appeared and disappeared. Blue line indicates GOES 0.5-4~Å flux.

ure 9), with the exception of a stretching factor of approximately two. If we scale the reconstructed magnetic field, the positions of the bright stripe and the separator coincide.

The discrepancy between the TESIS images and the reconstructed magnetic field can be explained by several reasons. First, since the pre-erupting structure had the energy to erupt, its magnetic field must be non-potential and therefore cannot coincide with the potential field obtained with the PFSS method. The second reason is the time lag between the magnetogram and the TESIS images. In fact, the part of the PFSS field map containing the magnetogram of the AR was taken at the moment of crossing the central meridian (see Figure 8), i.e., in an early phase of its evolution, after which the AR strength may have increased. Finally, the deviation of the model parameters (such as the height of the source surface) and the contribution of high-order harmonics in the PFSS method could also affect the result.

3.3. STEREO Observations

In the low corona, the CME pre-eruption structure was a sheared arcade, which was seen on the EUVI-A 284 Å images (see Figure 10). In other EUVI channels the sheared arcade was less distinctive. To determine a shear angle, we measured coordinates of the arcade footpoints (points P, A, and B in Figure 10.) Assuming that these points lie on the solar surface, we obtained 3D coordinates of the vectors \overrightarrow{PA} and \overrightarrow{PB} , and then determine the angle β (see Figure 10). To estimate error bars, we repeated this procedure 25 times. We obtained that $\beta = 40 \pm 4^{\circ}$, that is, the arcade is indeed sheared.

Loops of the arcade slowly moved up (see Figure 11). As the loops moved up, their intensity decreased. At 13:36 UT, the CME appeared on the EUVI running difference images (see Figure 12). At 15:26 UT, a flare arcade appeared on the EUVI 284 Å images.

To determine when the loops of the arcade started to move up, we made the stack-plot of slices, cut from running difference EUVI-A 284 Å images. The positions of the slices are indicated in Figure 11. All slices were cut in the radial direction. The position of the slices were differentially rotated for each image, in order to exclude rotation of the Sun from the analysis.

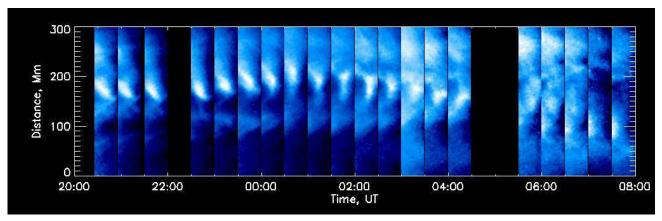


Figure 6. Stack plot of the slices, which were cut from TESIS images in the vicinity of the X-point. Position of the slices is indicated on the Figure 3. The width of the slices is 60'' (44 Mm).

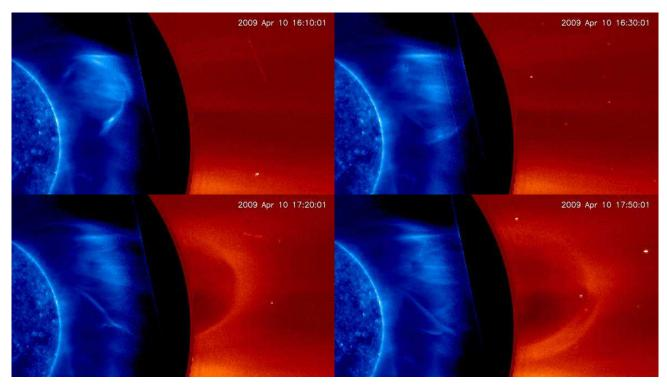


Figure 7. CME. Blue: TESIS 171 Å images; red: LASCO/C2 images. The video is available for this figure.

On the obtained stack-plot, we see several dark linear features (see Figure 13). These features correspond to the expanding loops. We marked the two most distinctive features with green and yellow lines. Their speeds lie in the range of 1–6 km s⁻¹ (values are obtained from linear fitting). The motion started at $\approx 01{:}45$ UT (almost at the same time that the bright stripe appeared).

On the COR2 images, the CME had a three-part structure: bright core, dark cavity, and bright frontal loop (see Figure 14). The core, which is usually interpreted as a prominence, was not seen on the TESIS and EUVI images.

3.4. Kinematics

The CME was observed by TESIS, EUVI, COR2, and LASCO. These instruments cover different distance ranges, and it is possible to study CME kinematics from

the solar surface up to the boundaries of the LASCO C3 field of view. However, this research should be carried out with caution. TESIS and *STEREO-A* EUVI observe thermal emission of plasma with different temperatures, while COR2 and LASCO observe scattered light. We should be careful to ensure that we measure kinematics of the same part of the CME. In this research, we will study kinematics of the CME frontal loop.

We used running difference images to measure frontal loop coordinates on the TESIS and EUVI images, and normal images on LASCO and COR2. The measurement was carried out by a simple point-and-click procedure. To estimate error bars, we repeated the procedure 9 times. The result of the kinematics measured on EUVI images is shown in Figure 15. The curves in different channels deviate from one another because different channels have different temperature response functions

and we measure slightly different parts of the CME.

To fix this deviation, we propose the following model. We assume that all parts of the CME expanded proportionally. If h(t) and h'(t) are heights of different parts of the CME (see Figure 16), we assume that

$$h'(t) = \alpha h(t), \tag{1}$$

where $\alpha=const.$ We can rewrite equation (1) using radial coordinates (distance from the Sun's center on the image):

$$r' - r_0 = \alpha(r - r_0) \tag{2}$$

$$r' = \alpha(r - r_0) + r_0, (3)$$

where r_0 is the radial coordinate of the CME footpoints, and r' and r are radial coordinates of CME parts observed in different channels. We scaled channels 284 Å and 171 Å using formula (3) to match the curve of the 195 Å channel. For 284 Å we used $\alpha = 1.26$, and $\alpha = 1.05$ for 171 Å. The scaled curve fit the 195 Å curve well, which shows that our model is reasonable.

The TESIS and LASCO line of sight was inclined by 46° to the *STEREO-A* line of sight (see Figure 2). The CME trajectory was inclined by approximately the same angle to the TESIS/LASCO and *STEREO-A* image planes. That is why TESIS and LASCO kinematics curves almost coincide with EUVI and COR2 curves. To make the correspondence better, we multiplied TESIS coordinates by 0.99, LASCO/C2 by 1.02, and LASCO/C3 by 1.11. This correction accounts for different projection angles and the fact that different instruments observed different parts of the CME. After the correction, all data fit perfectly. We numerically differentiated the height-time profile and obtained CME velocity and acceleration (see Figures 17 and 18).

To determine timing of the CME acceleration, we ap-

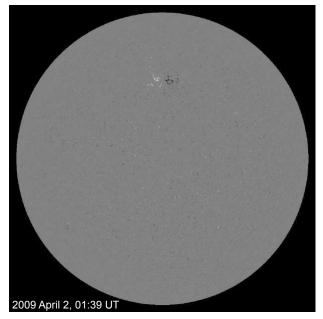


Figure 8. Magnetogram taken by MDI on April 2, 2009.

proximated r(t) with the formula (Sheeley et al. 2007)

$$r(t) = r_1 + \frac{v_f + v_0}{2}(t - t_1) + \frac{v_f - v_0}{2}\tau \ln \cosh\left(\frac{t - t_1}{\tau}\right),$$
(4)

where t_1 —time of the maximum acceleration; τ —acceleration timescale; v_0 —initial CME velocity; v_f —final CME velocity; and r_1 —CME position at $t=t_1$ $(r_1=r(t_1))$.

We differentiated equation (4) and calculated velocity and acceleration. The result of the approximation is plotted in Figures 17 and 18. As we see, formula (4) describes kinematics well up to 5 R_{\odot} . The CME is impulsively accelerated from 15:10 until 15:50 UT. The peak acceleration was 85 m s⁻², the velocity before impulsive acceleration was 7 km s⁻¹, and the velocity after impulsive acceleration was 155 km s⁻¹. During impulsive acceleration, a flare arcade appeared on the EUVI 284 Å images (see Figures 17 and 12).

At distances above 7 R_{\odot} the CME accelerated up to 350 km s⁻¹ over \approx 7 hours with acceleration \approx 10 m s⁻². The CME trajectory was inclined by approximately 23° to image planes. This means that real values of velocities and accelerations should be 8 % higher.

3.5. Summary of the Observations

We will briefly summarize the observations.

- 1. EUVI-A 284 Å observed a sheared arcade.
- 2. From 12:00 UT April 8 until 21:45 UT on 2009 April 9, TESIS observed quadrupolar structure.
- 3. A reconstructed from the MDI data magnetic field has a multipolar structure with an X-point above the AR.
- 4. From 21:45 UT April 9 until 01:15 UT on 2009 April 10, loops near the X-point moved away from each other.
- 5. At 01:15 UT, a bright stripe appeared between the loops. At 04:15 UT, the bright stripe disappeared.
- 6. From 01:45 to 04:30 UT, the flux in the GOES 0.5–4 Å channel increased.
- 7. At 01:45 UT, loops below the X-point started to slowly move up on the EUVI-A 284 Å images.
- 8. From 15:10 UT to 15:50 UT, the CME impulsively accelerated.
- 9. At 15:26 UT, a flare arcade appeared on the EUVIA 284 Å images.
- 10. From 15:50 UT to 19:00 UT, the CME moved with constant velocity.
- 11. After 19:00 UT, the CME slowly accelerated up to 350 km $\rm s^{-1}.$

The timing of the observations is illustrated in Figure 19.

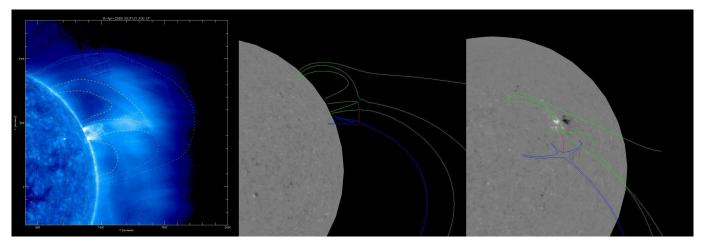


Figure 9. Left: TESIS image; middle: reconstructed magnetic field, TESIS point of view; right: reconstructed magnetic field, behind-the-limb point of view. Blue: the field lines adjacent to the null-point; red: the separator field line originating from the null; green: other field lines.

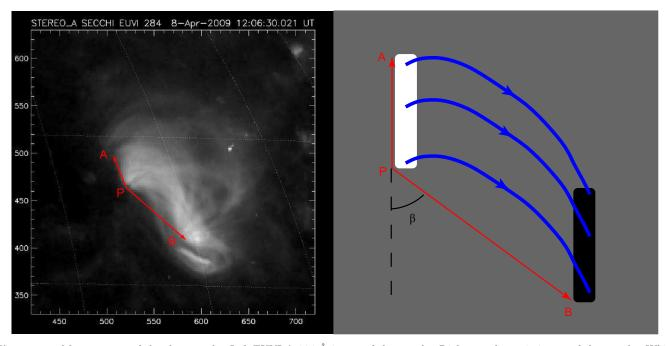


Figure 10. Measurement of the shear angle. Left:EUVI-A 284 Å image of the arcade. Right: a schematic image of the arcade. White indicates positive polarity; black—negative; gray—neutral.

4. DISCUSSION

4.1. Breakout Model and Observations

We presented observations of the CME in the far corona, which showed evidence of the breakout model. Below we will compare the breakout scenario with the observations.

1. Model: The CME pre-eruption structure should be quadrupolar.

Observations: The AR pre-eruptive configuration was quadrupolar on the TESIS Fe 171 Å images. Since magnetic field lines are lightened on the Fe 171 Å images, we interpret the observed structure as a magnetic quadrupolar structure. Also, a reconstructed from the MDI data magnetic field has a multipolar structure with an X-point above the AR.

- 2. *Model*: The driving mechanism for the eruption is the shearing motion of the arcade footpoints, which lie below the X-point.
 - Observations: We observed a sheared arcade on the EUVI-A 284 Å images. The sheared arcade is seen most distinctively during and after the CME impulsive acceleration.
- 3. Model: The shearing arcade motion should eventually lead to the stretching of the X-point into the current sheet. When the current sheet is stretched enough, the breakout reconnection occurs.

Observations: We see that loops, which formed the X-point, moved away from each other. The movement of the loops near the X-point stopped for ≈ 3 hours, a bright stripe appeared between them, and a GOES flux in the 0.5–4 Å channel increased. We interpret the loop motion and the stripe as ev-

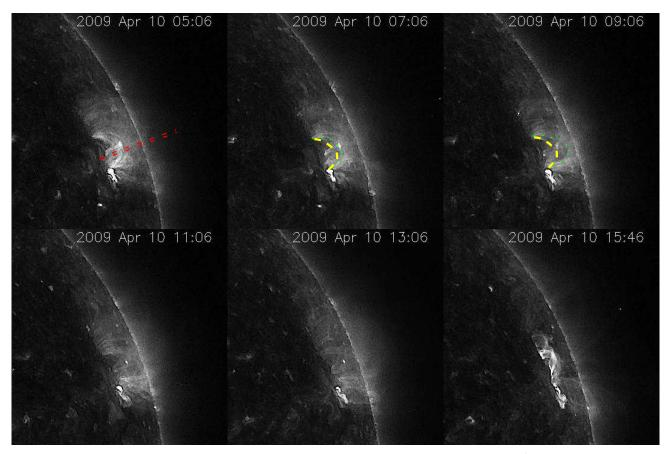


Figure 11. Slow upward motion of the loops of the CME arcade. These are sharpened STEREO-A 284 Å images, which were taken on April 10, 2009. Dashed yellow lines indicate positions of the loop at 05:06 UT. Green dotted lines indicate positions of the loop at the time the image was taken. Red dashed lines indicate the position of the slices, which were used in the construction of the Figure 13.

idence of the breakout reconnection.

- 4. *Model*: After the breakout reconnection, the CME should start to slowly move up. *Observations*: We see slow upward loop motion on the EUVI-A 284 Å images.
- 5. Model: The slow CME motion should stretch a current sheet below it. This will cause a flare and an impulsive CME acceleration. Observations: We see simultaneous impulsive CME acceleration and a flare arcade around 15:26 UT on the EUVI-A 284 Å images.
- 6. Model: After the impulsive acceleration ends, CME should move with constant velocity. Observations: After the impulsive acceleration, the CME moved with constant velocity.

The comparison is summarized in Table 1. The observed CME explicitly followed the breakout model scenario: quadrupolar structure, sheared arcade, breakout reconnection, simultaneous impulsive acceleration and a flare, and the CME kinematics. The main result of our work is the observation of the key element of the model—the breakout reconnection.

4.2. Bright Stripe

In flares during reconnection, plasma is heated up to 10 MK. Such hot plasma should be seen as a darkening in the 171 Å line. In our observations, however, we see brightening. We found two ways to explain why the stripe is bright, but not dark.

The loops near the X-point moved slowly, and corresponding reconnection should also be slow. The magnetic field of the AR was weak. In these circumstances, the reconnection rate could be sufficient to heat plasma to temperatures of only around 1 MK. In this case, the current sheet should be seen as a brightening in the 171 Å line.

An alternative explanation is that we see an increase in density. During reconnection, plasma inflows from areas surrounding the current sheet increase the current-sheet density. Also, at high altitudes, scattering—which depends on density—contributes to the emission in the 171 Å line (Reva et al. 2014). It is possible that the observed bright stripe is the scattered light in the dense current sheet.

There are also few observations in which a brightening in the 171 Å line was interpreted as a reconnection. Masson et al. (2014) analyzed the pseudostreamer observed by Atmospheric Imaging Assembly (AIA Lemen et al. 2011), and van Driel-Gesztelyi et al. (2014) analyzed an active region near the area of the expanding CME observed by AIA. Both authors reconstructed magnetic fields using Helioseismic and Magnetic

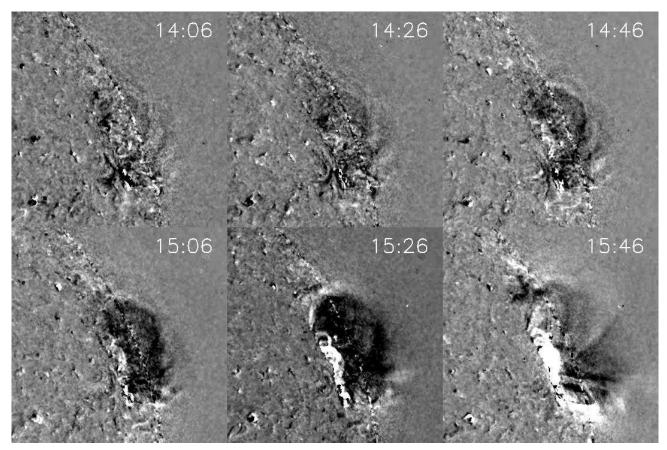


Figure 12. STEREO-A 284 Å images running difference images. Images were taken on April 10, 2009.

 ${\bf Table~1}$ Comparison of the breakout model and the observations

Model	Observations	Instrument
Quadrupolar pre-erupting magnetic structure	Quadrupolar pre-erupting structure	TESIS Fe 171 Å
	Reconstructed magnetic field	MDI
Shearing arcade motion	Sheared arcade	EUVI-A 284 Å
Breakout reconnection	Loops moved away from each other near the X-point	TESIS Fe 171 $ ext{Å}$
	Bright stripe	TESIS Fe 171 $ ext{Å}$
Slow CME acceleration	Slow loop upward motion	EUVI-A 284 Å
Flare	Post-flare arcade	EUVI-A 284 Å
Impulsive CME acceleration	Impulsive CME acceleration	Kinematics
Propagation with a constant velocity	Propagation with a constant velocity	Kinematics

Imager data (HMI, Schou et al. (2012)), and showed that there was a brightening in the 171 Å line near the magnetic null-point. Both authors interpreted brightening as a reconnection in the current sheet.

Although the bright stripe looks like a current sheet, it could occur due to other reasons: plasma compression; plasma heating or cooling to the formation temperature of the Fe 171 Å line; or a chance alignment of several structures along the line of sight during the magnetic field reconfiguration. However, the bright stripe was accompanied by other evidence of the reconnection—the sideways loop motion. The bright stripe could be explained in the reconnection framework. There are observations where brightening in the 171 Å line was interpreted as a reconnection in the current sheet. We think that our interpretation of the bright stripe as a reconnection in the current sheet is a reasonable conclusion.

4.3. GOES Signal

When the bright stripe appeared, the GOES flux increased. Although, it is tempting to interpret the GOES signal as an indirect evidence of the breakout reconnection, we cannot prove the connection between the bright stripe and the increase in the GOES flux. GOES do not have imaging capabilities, and the flux increase could be just a coincidence. The signal was very weak, and it could come from other parts of the Sun. However, even if the GOES signal was not related to the breakout reconnection, it is still a useful information. It provides a higher estimate on the possible soft-X-ray flux from the breakout reconnection region.

During eruption, the source AR for the analyzed CME was behind the solar limb, as seen from the terrestrial viewpoint. This makes it impossible to use the GOES data to find the class of the associated flare.

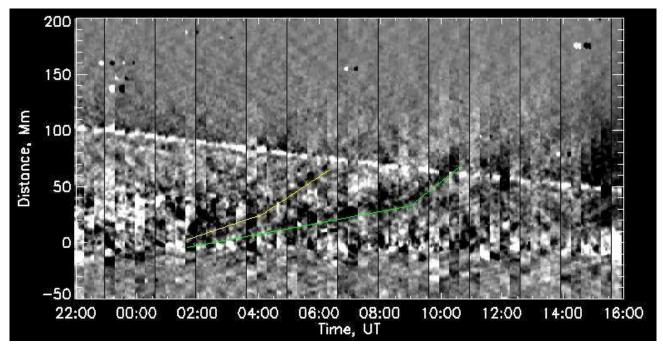


Figure 13. Stack-plot of slices, which were cut from running difference images of STEREO-A 284 Å. Green and yellow lines indicate loops moving upwards. Position of the slices is indicated in Figure 11. The width of the slices is 10" (7.2 Mm).

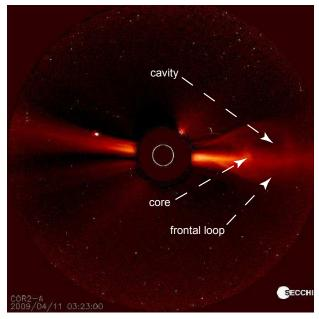


Figure 14. CME three-part structure.

4.4. Timing of the CME and the Breakout Reconnection

According to our observations, the breakout reconnection occurred from 01:15 UT to 04:15 UT, and the impulsive acceleration began at 15:10 UT. Such a long delay (11 hr) looks unusual and deserves discussion. In this section, we will compare the delay with previous observations of the evidence of the breakout reconnection, numerical simulations, and kinematics timing.

Manoharan & Kundu (2003); Aurass et al. (2011, 2013) observed evidence of breakout reconnection in radio data 1–5 minutes before the CME. Gary & Moore

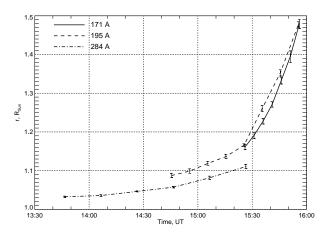


Figure 15. Radial coordinates of the front edges in different *STEREO-A* EUVI channels. Solid line: 171 Å channel; dashed line: 195 Å channel; dashed dotted line: 284 Å channel.

(2004) observed brightenings (which authors interpreted as a breakout reconnection) 4 minutes before the CME. Sterling & Moore (2001) observed 'EIT crinkles' 40–50 minutes before the CME. Sterling & Moore (2004a) observed pre-eruption dimming 6 hr before CME. We see that, in previous observations, the delay between the breakout reconnection and the CME ranges from a few minutes to 6 hr.

In numerical simulations, the delay between breakout reconnection and impulsive CME acceleration encompasses a wide range of possible values: 10 minutes in Lynch et al. (2005), 15 minutes in Masson et al. (2013), 8 hr in Karpen et al. (2012), and 13 hr in (Zuccarello et al. 2008). The delay observed in our work is consistent with the delay in the numerical simulations.

There is also another indirect way to check the reasonableness of the observed delay. In the breakout model,

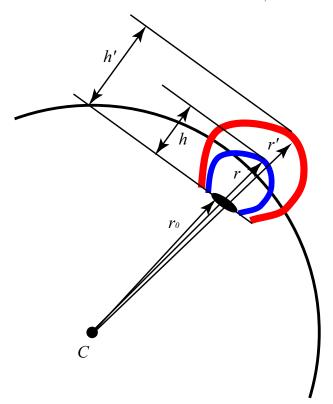


Figure 16. Scaling of different EUVI channels.

the CME has three phase kinematics: slow acceleration (after breakout reconnection and before flare reconnection), impulsive acceleration (during flare reconnection), and propagation with constant velocity (after flare reconnection). If we assume that the observed in CMEs three phase kinematics is caused by the breakout scenario, then we can use the delay between the CME onset and the start of the impulsive acceleration as an estimate of the delay between breakout and flare reconnections. Alissandrakis et al. (2013) reported a 15-minutes delay, Zhang et al. (2001) reported a 1-1.5-hr delay, Lin et al. (2010) reported a 4-hr delay, and Reva et al. (2014) reported a 12-hr delay. The delay in kinematics phases ranges from 15 minutes to 12 hours.

As we see, the delay between the breakout reconnection and the impulsive acceleration observed in our work is consistent with previous observations, numerical simulations, and CME kinematics timing. The delay ranges from several minutes to 13 hr. We think that the value of the delay is determined by the rate at which the energy is pumped into the system. The observed CME occurred during the deep minimum of the solar cycle. We think that the delay was long because at that time the energy pumping rate was low. Also, since for some CMEs breakout reconnection occurs few hours before eruption, the TESIS-like observations of the breakout reconnection could be used to forecast CMEs.

4.5. Additional Acceleration

Below 5 R_{\odot} the CME had three phase kinematics, which is consistent with the breakout model. Above 5 R_{\odot} the CME experienced additional acceleration from 150 to 350 km s⁻¹. The breakout model describes the CME initiation, and the details of the CME propagation lie be-

yond the scope of the breakout model (Antiochos et al. 1999; Lynch et al. 2008). We need a different model to explain the additional CME acceleration.

Yashiro et al. (2004) showed that CMEs with a velocity greater than 400 km s $^{-1}$ decelerate, and CMEs with a velocity less than 400 km s $^{-1}$ accelerate. The authors proposed that fast CMEs move faster than the solar wind, and the wind decelerates them, while slow CMEs move slower than the solar wind, and the wind accelerates them.

The analyzed CME after breakout reconnection moved with a velocity $150~\rm km~s^{-1}$. It is less than solar wind velocity $(400~\rm km~s^{-1})$, so the wind should accelerate the CME. Furthermore, the asymptotic velocity of the CME is $350~\rm km~s^{-1}$, which is close to the solar wind velocity. We think that the additional acceleration of the analyzed CME was caused by the solar wind.

The breakout model describes CME initiation. The model of the CME acceleration by the solar wind describes CME propagation. Both models have their limitations: the breakout model cannot explain CME late evolution, while acceleration by the solar wind cannot explain CME initiation. Therefore, it is natural that the breakout model does not explain every aspect of the presented observations.

4.6. Data We Did Not Use

In this work, we used data from *STEREO-A*, TESIS, MDI, LASCO, and GOES. We tried to adapt data from other instruments to our research, but did not include them in the paper. Below we will list these instruments and explain why we excluded them from the research.

We wanted to find another independent way to prove the presence of the breakout reconnection. We looked into radio data. During the breakout reconnection, the Sun was observed by the Hiraiso Radio Spectrograph (Kondo et al. 1995). The radio intensity slightly increased from 00:00 UT to 03:00 UT on April 10, which could be interpreted as a sign of the breakout reconnection. However, we find this conclusion too speculative, and that is why we did not include radio data in our research.

It would be great to have RHESSI (Lin et al. 2002) imaging observations for the analyzed event. However, the X-ray flux from the Sun was very weak, and the RHESSI signal did not exceed the sensitivity threshold.

TESIS far corona images are available only in the Fe 171 Å line. It would be nice to complement TESIS images with far corona images in other wavelength. Sadly, other EUV and soft X-ray telescopes—for example, EIT (Delaboudinière et al. 1995) and XRT (Golub et al. 2007)—do not have enough dynamic range to register far corona. TESIS Fe 171 Å images were the only option to observe this event in the far corona.

5. CONCLUSION

We presented CME observations with a TESIS Fe 171 Å telescope. The telescope could observe corona up to $2 R_{\odot}$. It observed an AR with a quadrupolar structure. In this structure, loops, which formed an X-point, started to move away from each other. Some time later, a bright stripe appeared between the loops. When the bright stripe disappeared, the loops below the X-point

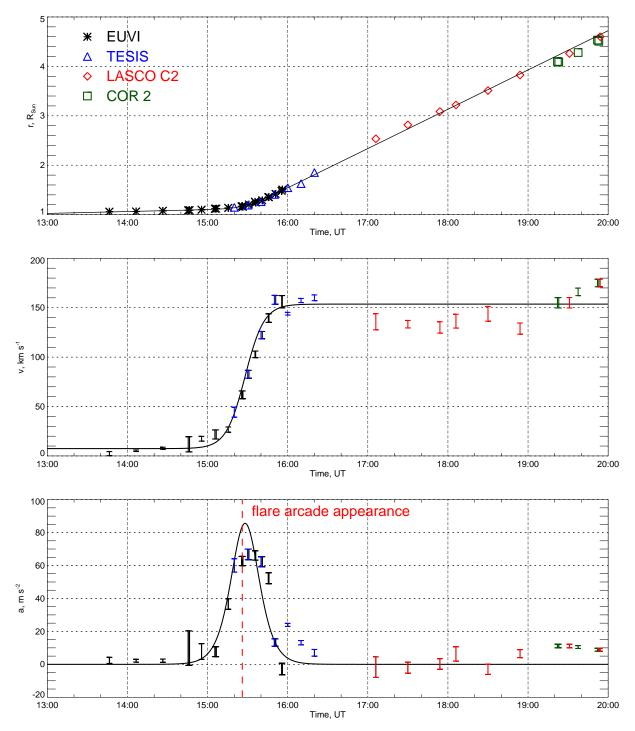


Figure 17. Combined CME kinematics. Top: radial coordinate of the CME front edge; middle: radial velocity; bottom: radial acceleration. Black stars: *STEREO-A* EUVI channels; blue triangle: TESIS EUV telescope; red diamond: LASCO C2; green square: *STEREO-A* COR2. Vertical dashed red line indicates appearance of flare arcade on the *STEREO-A* 284 Å images.

started to slowly move up. Some time later, the CME erupted and a flare arcade formed below it.

We interpreted this event in terms of the breakout model. We think that quadrupolar pre-erupting structure is a breakout pre-CME structure, and loop motions near X-point and the bright stripe are evidence of the breakout reconnection. CME evolution precisely followed the breakout scenario. In our opinion, the presented ob-

servations are valuable evidence of the breakout model.

We are grateful to Brigitte Schmieder for her valuable advice. This work was supported by a grant from the Russian Foundation of Basic Research (grant 14-02-00945) and by Program No. 9 for fundamental research

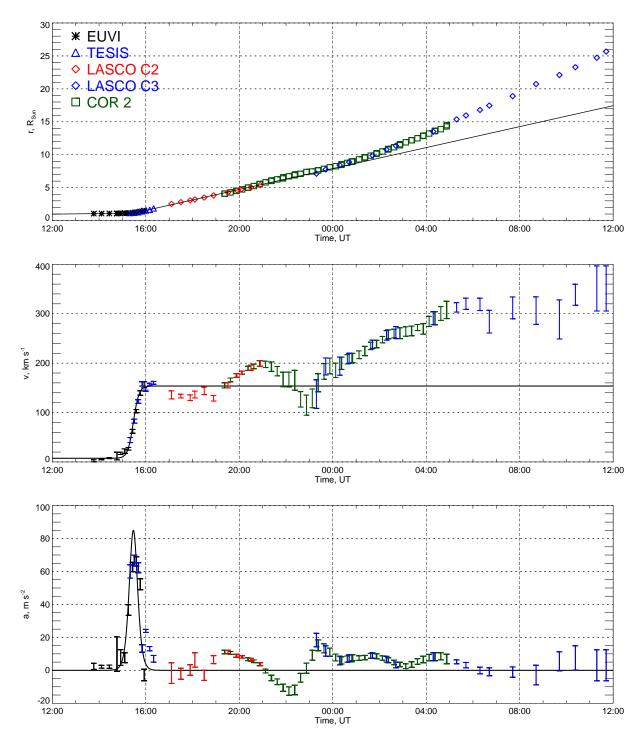


Figure 18. Combined CME kinematics. Top: radial coordinate of the CME front edge; middle: radial velocity; bottom: radial acceleration. Black stars: STEREO-A EUVI channels; blue triangle: TESIS EUV telescope; red diamond: LASCO C2; blue diamond: LASCO C3; green square: STEREO-A COR2.

of the Presidium of the Russian Academy of Sciences.

REFERENCES

Alissandrakis, C. E., Kochanov, A. A., Patsourakos, S., et al. 2013, PASJ, 65, 8
Aly, J. J. 1984, ApJ, 283, 349
Antiochos, S. K., DeVore, C. R., & Klimchuk, J. A. 1999, ApJ,

510, 485

Aulanier, G., DeLuca, E. E., Antiochos, S. K., McMullen, R. A., & Golub, L. 2000, ApJ, 540, 1126

Aurass, H., Holman, G., Braune, S., Mann, G., & Zlobec, P. 2013, A&A, 555, A40 Aurass, H., Mann, G., Zlobec, P., & Karlický, M. 2011, ApJ, 730,

St
Bemporad, A., Raymond, J., Poletto, G., & Romoli, M. 2007, ApJ, 655, 576
Brueckner, G. E., Howard, R. A., Koomen, M. J., et al. 1995, Sol. Phys., 162, 357
Carmichael, H. 1964, NASA Special Publication, 50, 451
Delaboudinière, J., Artzner, G. E., Brunaud, J., et al. 1995, Sol. Phys., 162, 291

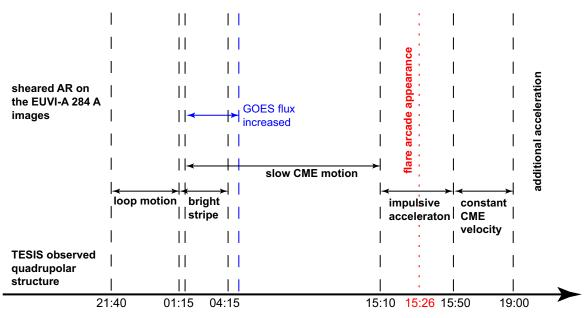


Figure 19. Timing of the observations.

Domingo, V., Fleck, B., & Poland, A. I. 1995, Sol. Phys., 162, 1 Gary, G. A., & Moore, R. L. 2004, ApJ, 611, 545 Golub, L., Deluca, E., Austin, G., et al. 2007, Sol. Phys., 243, 63 Hirayama, T. 1974, Sol. Phys., 34, 323 Howard, R. A., Moses, J. D., Vourlidas, A., et al. 2008, Space Sci. Rev., 136, 67

Karpen, J. T., Antiochos, S. K., & DeVore, C. R. 2012, ApJ, 760,

81
Kondo, T., Isobe, T., Igi, S., Watari, S., & Tokimura, M. 1995,
J. Commun. Res. Lab., Vol. 42, No. 1, p. 111–119, 42, 111
Kopp, R. A., & Pneuman, G. W. 1976, Sol. Phys., 50, 85
Kotov, Y. D. 2011, Solar System Research, 45, 93
Kuzin, S. V., Zhitnik, I. A., Shestov, S. V., et al. 2011, Solar System Research, 45, 162
Lemen, J. R., Title, A. M., Akin, D. J., et al. 2011, Sol. Phys., 172
Lin, C.-H., Gallagher, P. T., & Raftery, C. L. 2010, A&A, 516, A44

Lin, R. P., Dennis, B. R., Hurford, G. J., et al. 2002, Sol. Phys., 210, 3

Lynch, B. J., Antiochos, S. K., de Vore, C. R., & Zurbuchen, T. H. 2005, in ESA Special Publication, Vol. 592, Solar Wind 11/SOHO 16, Connecting Sun and Heliosphere, ed. B. Fleck,

T. H. Zurbuchen, & H. Lacoste, 297 Lynch, B. J., Antiochos, S. K., DeVore, C. R., Luhmann, J. G., & Zurbuchen, T. H. 2008, ApJ, 683, 1192 Mackay, D., & Yeates, A. 2012, Living Reviews in Solar Physics,

MacNeice, P., Antiochos, S. K., Phillips, A., et al. 2004, ApJ, 614,

Manoharan, P. K., & Kundu, M. R. 2003, ApJ, 592, 597

Masson, S., Antiochos, S. K., & DeVore, C. R. 2013, ApJ, 771, 82 Masson, S., McCauley, P., Golub, L., Reeves, K. K., & DeLuca, E. E. 2014, ApJ, 787, 145
Pulkkinen, T. 2007, Living Reviews in Solar Physics, 4
Reva, A. A., Ulyanov, A. S., Bogachev, S. A., & Kuzin, S. V. 2014, ApJ, 793, 140
Scherrer, P. H., Bogart, R. S., Bush, R. I., et al. 1995, Sol. Phys., 162, 129
Schou, J. Scherrer, P. H., Brief, P. J. 1995, Schott F. Scherrer, P. H., Brief, R. J. 1995, Sol. Phys., 162, 129

Schou, J., Scherrer, P. H., Bush, R. I., et al. 2012, Sol. Phys., 275,

Schwenn, R. 2006, Living Reviews in Solar Physics, 3 Seaton, D. B., Berghmans, D., Nicula, B., et al. 2013, Sol. Phys., 286, 43

250, 450, Sheeley, Jr., N. R., Warren, H. P., & Wang, Y.-M. 2007, ApJ, 671, 926

Sterling, A. C., & Moore, R. L. 2001, ApJ, 560, 1045

— 2004a, ApJ, 602, 1024

— 2004b, ApJ, 613, 1221
Sturrock, P. A. 1966, Nature, 211, 695

— 1991, ApJ, 380, 655

van Driel-Gesztelyi, L., Baker, D., Török, T., et al. 2014, ApJ,

Yashiro, S., Gopalswamy, N., Michalek, G., et al. 2004, Journal of Geophysical Research (Space Physics), 109, 7105

Zhang, J., Dere, K. P., Howard, R. A., Kundu, M. R., & White,
S. M. 2001, ApJ, 559, 452
Zuccarello, F. P., Soenen, A., Poedts, S., Zuccarello, F., & Jacobs,
C. 2008, ApJL, 689, L157